The Radial HMF in Fast and Slow Solar Wind

X. P. Zhao and J. T. Hoeksema

Stanford University, Stanford, CA 94305

Abstract. From Ulysses observations of magnetic field and plasma properties during its rapid pole-to-pole scan, we determine the causes of variations in the magnitude of the radial component of the heliospheric magnetic field (HMF). We find that the ambient radial HMF in the slow solar wind is a combination of the ambient radial HMF components of the two hemispheres with opposite polarities. It suggests that the source region of the slow solar wind has the same magnetic topology as the source region of the fast solar wind, i.e., both are open field regions.

INTRODUCTION

The slow solar wind, found near the heliospheric current sheet, differs from the fast solar wind not only in its plasma properties, but also in composition and variability. The differences have been explained as signatures of coronal streamers in the heliosphere (4). However, comparison of Ulysses observations with coronal hole observations and coronal magnetic field models, indicates that almost all the wind with speed less than $600 kms^{-1}$ originates in smaller coronal holes at low latitudes or in open field regions near the equatorward borders of polar coronal holes (see Table 2 and Figure 5 of (6)).

The radial component of the HMF, B_r, is a characteristic property of the solar magnetic field (11). According to the Parker's HMF model the magnetic flux for $B_r$is a constant, i.e., $R^2 B_r = B_{r1au}$. Here R denotes the heliocentric distance in AU and $B_r$and B_{r1au} the radial HMF components at R and 1 AU. The B_{r1au} in slow solar wind is expected to be different from the B_{r1au} in north and south fast solar wind if the source of the slow solar wind is coronal helmet streamers, rather than coronal holes. Therefore comparing B_{r1au} in slow wind with B_{r1au} in fast wind may provide some clue for determining whether or not the slow solar wind originates in closed field regions, open field regions, or within the boundary layer between the northern and southern hemispheres with opposite magnetic polarities.

The 3-rotation average of Ulysses B_{r1au} in the southern hemisphere is nearly the same as the 3-rotation average of near-ecliptic IMP-8 B_r that has the same polarity as the B_{r1au} in the southern hemisphere (9). The solar source of all the solar wind near the ecliptic was implicitly assumed in that work to be polar coronal holes.

The Ulysses data, with its very small measurement error of 4.0 pT (2), observed during its rapid latitude scan (Figure 1) provide a rare opportunity to derive and compare the ambient B_{r1au} in the fast and slow solar wind.

DATA

Panels A and B of Figure 1 on the following page show the hourly proton bulk speed and the normalized radial HMF, B_{r1au}, during the rapid pole-to-pole scan. All Ulysses data used in this paper were downloaded from the COHOWeb. They were observed by the ion and electron spectrometers of the Ulysses solar wind plasma experiment (1) and by the Vector Helium magnetometer (2). A few special events are indicated by vertical lines in Panel A. In the polar wind a coronal mass ejection (between the two dashed lines) and two non-CME driven reverse shocks (the outer dotted-dashed lines) were observed. At lower latitude one non-CME driven forward shock (the middle dotted-dashed line) was observed (7).

The observed B_{r1au} includes various temporal and spatial variations. Solar cycle variations of both the solar and the heliospheric magnetic fields are expected to be negligible in an interval less than a year near solar minimum (3). To avoid the effects of fast and slow stream-stream interactions, we specifically define as "slow" the solar wind with proton bulk speed less than $450 kms^{-1}$ (7) and consider wind speedier than $700 kms^{-1}$ "fast." The two vertical dotted lines in Panel B indicate the times when Ulysses encountered the first and last slow so-

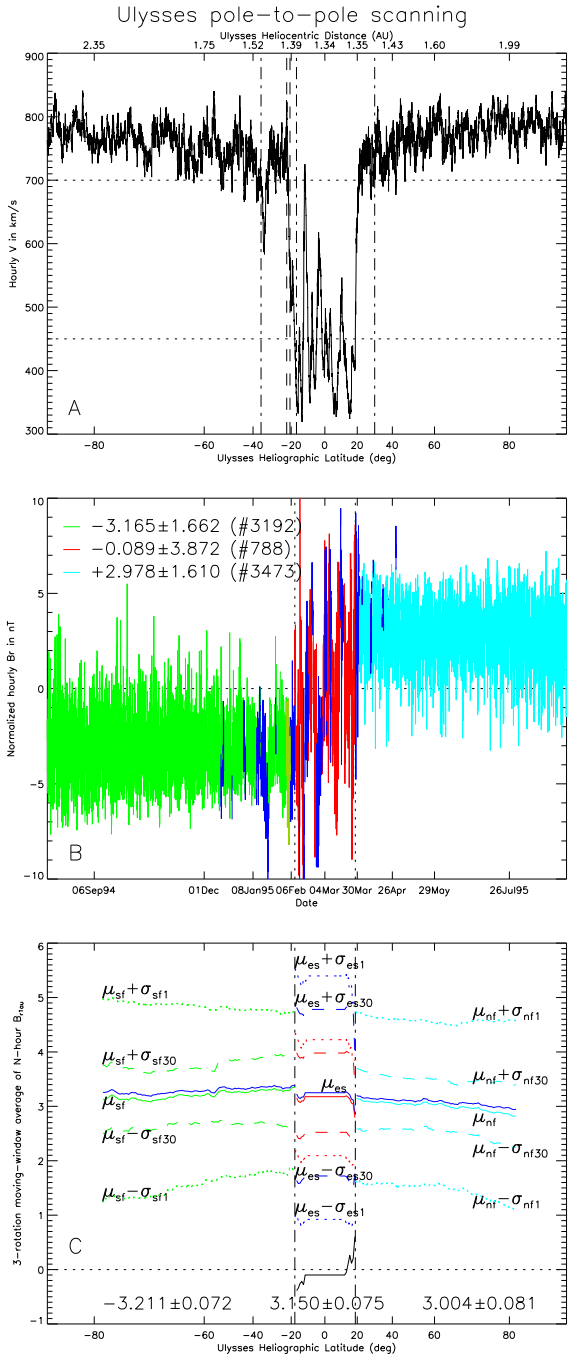

FIGURE 1. Ulysses observations of the solar wind velocity (panel A), the normalized radial component of the HMF B_{r1au} (panel B), and the 3-rotation averages of B_{r1au} (panel C).

lar wind, as defined here. The field values are color coded to indicate the wind speed. From Panels A and B one can see that the non-CME forward shock occurred in medium-speed solar wind and that the two non-CME reverse shocks in the fast wind were very weak; the change in B_{r1au} associated with the shocks was not dramatic and lasted only a few hours.

The frequent occurrence of opposite polarity B_{r1au} in the fast wind intervals (see Panel B) implies the existence of MHD fluctuations, specifically large-amplitude Alfven waves. Thus, on the short term, the ambient B_{r1au} will be contaminated primarily by MHD fluctuations and occasionally disturbed by CMEs.

The magnitude of the ambient B_{r1au} in the fast solar wind is nearly independent of latitude (3). Thus a part of the change in B_{r1au} must to some degree be caused by variations with heliographic longitude.

Because of the various variations superposed on the ambient or structureless B_{r1au}, although the measurement uncertainty is extremely small, the standard deviation of observed hourly B_{r1au} is expected to be very large relative to the mean, as shown in Panel B (The number of sample points used for each calculation is shown in parentheses). No meaningful comparison can be made between the ambient B_{r1au} in fast and slow solar wind. Any conclusion derived in this simple way, would be questionable (5). To infer the magnetic characteristics of the source of slow solar wind, what we need to compare is the heliolongitude-independent ambient B_{r1au} in the fast and slow solar wind.

ANALYSIS AND RESULTS

The effects of both MHD fluctuations and heliolongitude dependence on the ambient B_{r1au} are quasi-periodic. The longitude-independent ambient B_{r1au} in the period studied here may be assumed to be constant or changing linearly with time. Thus a moving window averaging procedure (8) with a width of three solar rotations may be used to filter out the effects of those quasi-periodic variations with no bias being introduced into the result. The effects of those features on the B_{r1au} can be estimated as follows.

Panel C shows the results calculated using observed hourly B_{r1au}. Data associated with the 3-5 February 1995 CME are excluded, as are all intervals of intermediate-speed solar wind. The mean and standard deviation, μ and σ, are calculated for a 3-rotation window centered at each specified hour; at least one third of hours in the window must have data.

The southern fast-wind mean values, μ_{sf}, are shown in green and lie to the left of the vertical lines; northern fast-wind values in light blue are to

the right (μ_{nf}). The spread is also shown by plotting $\mu_{sf} \pm \sigma_{sf1}$ and $\mu_{nf1} \pm \sigma_{nf1}$ with a dotted line.

The longitude-independent ambient B_{r1au} value is given by μ_{sf} or μ_{nf} because the effects of the major contaminating features mentioned above have been removed. The spread between the dotted lines indicates the variations within each 3-rotation window produced by MHD fluctuations, longitude dependence, measurement uncertainty, and other short term variations (9). The average σ_{sf1} (σ_{nf1}) is $\sim$ 1.64 nT ($\sim$ 1.56 nT) in the south (north) fast wind.

The period of Alfven waves ranges up to 10 hours (10). Averaging the observed hourly B_{r1au} over 30 hours may effectively filter out the effect of MHD fluctuations. The longitude-independent ambient B_{r1au} may then be derived by computing the 3-rotation moving window average of the 30-hour averaged B_{r1au}. The longitude-independent ambient B_{r1au} determined in this way should be the same as the solid lines if there were no data gaps. The negligible difference between them (not shown in Panel C) is the calculation error produced by data gaps. The dashed lines denoted by $\mu_{sf} \pm \sigma_{sf30}$ ($\mu_{nf} \pm \sigma_{nf30}$) display the spread of 30-hour averaged B_{r1au} around the longitude-independent ambient B_{r1au} for the south (north) fast wind. The average of σ_{sf30} (σ_{nf30}) is $\sim$ 0.56 nT ($\sim$ 0.50 nT) for the south (north) fast wind. The spread resulting from MHD fluctuations alone can thus be derived from $\sigma_{f1} - \sigma_{f30}$, which is $\sim$ 1.08 nT ($\sim$ 1.06 nT) for the south (north) fast wind.

Sector-like structures are easily seen in the sign of B_{r1au} in the slow wind in Panel B. To avoid cancellation of ambient B_{r1au} with opposite polarity when filtering out the effect of MHD fluctuations, averages of the magnitude of B_{r1au}, as well as the signed B_{r1au}, must be used. However using unsigned B_{r1au} will not completely filter out the effect of large-amplitude Alfven waves, and will introduce some error (when the Alfven fluctuation causes a change in polarity). The dark-blue solid lines located just above the solid lines denoted by μ_{sf} and μ_{nf} in Panel C show the 3-rotation moving window average of unsigned B_{r1au}. The difference is the error mentioned above. The average of the unsigned values is about 0.075 nT larger for south fast wind and 0.071 nT larger for north fast wind. We assume that the average of the unsigned values is about 0.073 nT larger for the low-latitude slow wind.

We now consider the slow-wind interval between the vertical lines in Panel C. The 3-rotation moving window average of signed hourly B_{r1au} is slightly less than 0 (solid black) with an average value of $\sim$ -0.089 nT, as shown in Panel B. If the field in the slow solar wind comes from episodically opening coronal helmets underlying the helmet cusps, it would be highly unlikely to produce the sector-like structure seen in the sign of B_{r1au}, though it is not impossible for the ambient B_{r1au} to be zero.

The solid dark-blue line denoted by μ_{es} is the 3-rotation moving window average of the unsigned hourly B_{r1au}. The mean value for the slow-wind interval falls between the corresponding mean values of the averaged unsigned hourly B_{r1au} of the southern and northern fast solar wind intervals. The μ_{es} curve is slightly higher than the solid green and light-blue lines (the fast-wind interval averages of signed B_{r1au}). The corresponding calculated σ_{es1} and σ_{es30} for the slow wind (shown in blue) are much greater than those of the fast wind. The difference is mainly associated with the smaller number of data samples in the slow wind. The red dotted and dashed lines are obtained by multiplying σ_{es30} and σ_{es1} by $(788/3473)^{0.5}$. The two slow-wind curves are much closer, showing that the contribution of MHD fluctuations to the spread of B_{r1au} in slow wind is less than in fast wind. Furthermore, the normalized σ_{es30} is about the same as σ_{sf30} and σ_{nf30}, thus the contribution of the longitude-dependence (and probably other unknown features) to the spread of B_{r1au} is basically the same in slow wind as in fast wind.

The means and standard deviations of μ_{sf} and μ_{nf} are shown at the bottom of Panel C. Since the normalized variance of B_r in the equatorial band is similar to that in the high latitude regions (see Figure 7 of (3)), the effect of MHD fluctuations on B_r in the slow wind may not be neglected, though the effect is much less than in the fast wind and the Alfven wave power averaged over a solar rotation decreases abruptly below $\sim$ 30° latitude (10). The red solid line in Panel C denotes $\mu_{es} - 0.073$. Its average is 3.150 nT, just in between 3.211 for the south fast wind and 3.00 nT for the north fast wind.

The pollutive effect of CMEs on B_{r1au} can also be estimated. Unfortunately the effects of transient CMEs can not be removed completely, even by averaging over three solar rotations. The local effect of a CME is expanded to half of the window size around the time of the CME on each side due to the moving window averaging procedure. The mean $B_r 1au$ is increased locally by 0.036 nT for the 3-5 February 1997 CME. The effect of CMEs will be significantly increased if several CMEs occur in an averaging interval and must be taken into consideration.

SUMMARY AND DISCUSSION

The major sources of variations in the normalized radial HMF component, B_{r1au}, in the high speed solar wind are MHD fluctuations, specifically large-amplitude Alfven waves. Their contribution to the spread of observed B_{r1au} in the fast solar wind is estimated to be of order 1.1 nT, more than two thirds of the whole spread of 1.6 nT. The effect of longitude inhomogeneity and other short term variations (9) on B_r are estimated to be 0.5 nT, about one third of the whole spread.

After the effects of MHD fluctuations and longitude-dependent variations of B_{r1au} are filtered out using 3-rotation moving window averaging, the standard deviation of the longitude-independent ambient B_{r1au} becomes small relative to the ambient B_{r1au} itself, making it possible to compare the longitude-independent ambient B_{r1au} in fast and slow solar wind. We find that the structureless B_{r1au} in the fast southern hemisphere wind in 1994/95 was -3.21 ± 0.07 nT, greater than the 3.00 ± 0.08 nT seen in the northern hemisphere fast wind by -0.2 nT. The difference is significant compared to the standard deviations. The ambient B_{r1au} of 3.15 ± 0.08 nT in slow solar wind is just between the two values in fast wind. In addition, the average of signed B_{r1au} in slow wind (see Figure 1) is -0.09, about half of the -0.2 nT difference between the north and south.

It is not impossible to explain an ambient B_{r1au} value near zero if the field comes from episodically opened coronal helmets underlying helmet cusps. However, it is certainly hard to see why an episodically opening coronal helmet would produce the sector-like structure observed in the sign of B_{r1au}.

These results strongly suggest that the ambient B_{r1au} in the slow solar wind is simply the combination of the ambient B_{r1au} in south and north wind. Thus the source of slow solar wind is the same as the source of fast solar wind in magnetic nature.

Comparison of the observed B_{r1au} with the heliospheric current sheet inferred from WSO photospheric field observations also support this conclusion, because the change in sign of B_r in the slow wind is simply due to crossing of the heliospheric current sheet from one polarity region to another.

The profiles of plasma properties in the slow solar wind show the same relationship among the velocity, density and temperature as is observed in the fast solar wind, i.e., the density decreases and the temperature increases as the velocity increases. This may explain the difference of the density and temperature in the slow and fast solar wind.

The slow and fast solar wind also differ in composition and variability. A real challenge remains for solar wind modelers to reproduce these differences within coronal holes.

REFERENCES

1. Bame, S. J., et al., The Ulysses solar wind plasma experiment, *Astron. Astrophys., Supp. Ser., 92*, 237, 1992.
2. Balogh, A., Beek, T. J., Forsyth, R. J., Hedgecock, P. C., Marquedant, R.. J., Smith, E. J., Southwood, D. J., and Tsurutani, B. T., The magnetic investigation on the Ulysses mission: Instrumentation and preliminary scientific results, *Astron Astrophys. Suppl. Ser., 92*, 221, 1992.
3. Forsyth, R. J., Balogh, A., Horburg, T. S., Erdos, G., Smith, E. J., and Burton, M. E., The heliospheric magnetic field at solar minimum: Ulysses observations from pole to pole, *Astron. Astrophys., 316*, 287, 1996.
4. Gosling, J. T., Borrini, G., Asbridge, J. R., Bame, S. J., Feldman, W. C., and Hansen, R. T., Coronal streamers in the solar wind at 1 AU, *J. Geophys. Res., 86*, 5438, 1981.
5. Marsch, E. and Richter, A. K., *J. Geophys. Res., 89*, 6599, 1984.
6. Neugebauer, M., Forsyth, R. J., Galvin, A. B., Harvey, K. L., Hoeksema, J. T., Lazarus, A. J., Lepping, R. P., Linker, J. A., Mikic, Z., Steinberg, J. T., von Steiger, R., Wang, Y.-M., and Wimmer-Schweingruber, R. F., Spatial structure of the solar wind and comparisons with solar data and models, *J. Geophys. Res., 103*, 14,587, 1998.
7. Phillips, J. L., Bame, S. J., Barraclough, B. L., Feldman, W. C., Goldstein, B. E., Gosling, J. T., Hoogeveen, G. W., McComas, D. J., Neugebauer, M., and Suess, S. T., Ulysses solar wind plasma observations from pole to pole, *Geophys. Res. Lett., 22*, 3301, 1995.
8. Press, W. H., Teukoisky, S. A., Vettering, W. T., Flannery, B. P., *Numerical Recipes in C*, second edn, ambridge, 1992.
9. Smith, E. J. and Balogh, A., Ulysses observations of the radial magnetic field, *Geophys. Res. Lett., 22*, 3317, 1995.
10. Smith, E. J., Balogh, A., Neugebauer, M., and McComas, D., Ulysses observations of Alfven waves in the southern and northern solar hemispheres, *Geophys. Res. Lett., 22*, 3381, 1995.
11. Zhao, X. P. and J. T. Hoeksema, Prediction of interplanetary magnetic field strength, *J. Geophys. Res., 100*, 1933, 1995.